BROADLY TUNABLE FREE-ELECTRON LASER FOR FOUR-WAVE MIXING EXPERIMENTS WITH SOFT X-RAY PULSES

G. Marcus, SLAC, Menlo Park, CA 94025, USA
G. Penn, LBNL, Berkeley, CA 94720, USA
A. A. Zholents, ANL, Argonne, IL 60439, USA

Abstract

This paper examines a FEL design for the production of three soft x-ray pulses from a single electron beam suitable for four-wave mixing experiments. Independent control of the wavelength, timing and angle of incidence of the three ultra-short, ultra-intense pulses with exquisite synchronization is critical. A process of selective amplification where a chirped electron beam and a tapered undulator are used to isolate the gain region to only a short fraction of the electron beam is explored in detail. Numerical particle simulations are used to demonstrate the essential features of this scheme in the context of the LCLS-II design study.

INTRODUCTION

Hard and soft X-ray free-electron lasers (FELs) [1–4] have become essential tools for the investigation of dynamical systems as they have the ability to operate on the time and length scales natural to atomic and electronic motion in matter [5]. Many experiments envisioned for the exploration of the dynamical properties of matter, which leverage the unique capabilities of FEL facilities, will be based on a pump and probe technique. Extending this technique to include a broad variety of four-wave mixing (FWM) spectroscopies, which rely on the use of three fully coherent and independent pulses of light with unique carrier frequencies and wave vectors, is of critical importance.

A pathway for producing FEL pulses suitable for FWM experiments from a single electron beam has recently been proposed [6]. In that study, a process of selective amplification employing a strongly chirped electron beam and a tapered undulator is used to isolate the gain region of a self-amplified spontaneous emission (SASE) FEL allowing for a single longitudinally coherent pulse to amplify to saturation [7–9]. The taper also serves to suppress gain outside the chirped region, leaving the electron beam capable of producing additional radiation in a downstream FEL process. This energy modulation and undulator taper combination can be repeated in multiple stages to produce the three independent FEL pulses necessary for FWM experiments if a broad tuning range is necessary. Alternatively, a grating and mask can be used to split one of these large bandwidth pulses if two nearby frequencies are sufficient. A potential beamline for this scenario is shown in Figure 1.

This paper describes the electron beam energy modulation and undulator taper requirements for the production of longitudinally coherent FEL pulses from the selective amplification process in the context of the LCLS-II design study for photon energies of $E_\gamma = 250 - 1000$ eV. Numerical
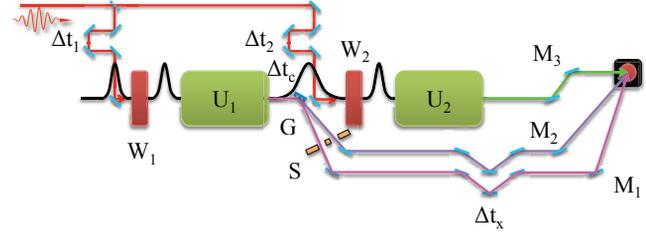
Figure 1: A possible beamline for a FWM FEL [6]: W_1 and W_2 are modulators, U_1 and U_2 are undulators, Δt_1 and Δt_2 are seed laser delay stages, Δt_c is the electron beam chicane delay, Δt_x is the x-ray delay line, G is the grating, S is the slit, and $M_{1,2,3}$ are adjustable x-ray mirrors.

simulations using the FEL code `GENESIS` [10] are used to illustrate the more impressive characteristics of this scheme at $E_\gamma = 1$ keV (see Table 1).

Table 1: Electron Beam, Undulator, and Modulator Laser Parameters for the Nominal LCLS-II Scenario

Paramter	Symbol	Value	Unit
e-beam energy	E	4.0	GeV
emittance	ϵ	0.45	mm-mrad
current	I	1000	A
energy spread	σ_E	500	keV
beta	$\langle \beta \rangle$	12	m
undulator period	λ_u	39	mm
segment length	L_u	3.4	m
break length	L_b	1.0	m
photon energy	E_γ	0.25 − 1	keV
seed wavelength	λ_s	2.1	μm

ELECTRON BEAM ENERGY CHIRP AND UNDULATOR TAPER

In the particular selective amplification scheme employed here, the electron beam is energy modulated by a carrier-envelope-phase-stable, single-cycle, mid-IR laser pulse within a single period modulator. This modulation takes the following idealized form [11]:

$$\gamma = \gamma_0 + \Delta\gamma \sin\left(\frac{2\pi}{\lambda_l}[s - s_0]\right) e^{-\frac{(s - s_0)^2}{2\sigma_l^2}}. \quad (1)$$
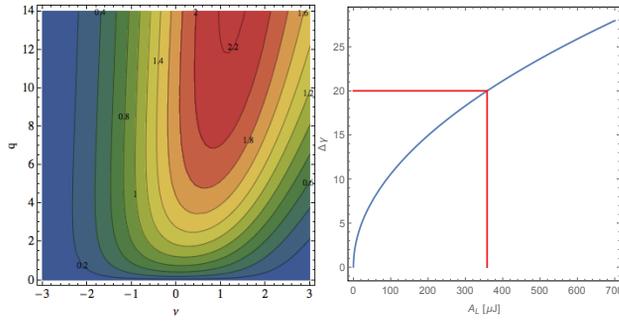
Figure 2: f as a function of q and ν for $\hat{\sigma}_\tau = 0.42$ (left) and $\Delta\gamma$ as a function of A_L for the optimized f (right).

Here, γ is the electron beam energy normalized to its rest energy (mc^2), λ_l is the seed laser wavelength, s is the electron coordinate with respect to the center of the bunch, σ_l is the rms width of the gaussian envelope for the single-cycle laser pulse longitudinal electric field and

$$\Delta\gamma = \frac{2}{mc^2}\sqrt{A_L \alpha \hbar \omega_0 \frac{K^2}{2+K^2}}\,[JJ]\,f\,(q,\nu,\hat{\sigma}_\tau)\,, \quad (2)$$

where A_L is the seed laser energy, α is the fine structure constant, $\hbar$ is Planck's constant, ω_0 is the mean frequency of the spontaneous radiation generated inside the modulator, $K = eB\lambda_u/2\pi mc$ is the undulator strength parameter, e is the electron charge, B is the peak magnetic field on axis, λ_u is the undulator period, $[JJ] = J_0\left[K^2/\left(4+2K^2\right)\right] - J_1\left[K^2/\left(4+2K^2\right)\right]$ is the Bessel form factor accounting for the coupling of electron motion to radiation emission in a planar undulator, and $f\,(q,\nu,\hat{\sigma}_\tau)$ depends in a complicated way on the undulator length, L_u, Rayleigh length ($q = L_u/z_R$), detuning ($\nu = 2L_u/\lambda_u(1-\gamma/\gamma_r)$), and the electric field pulse width ($\hat{\sigma}_\tau = \sigma_l \lambda_u/L_u\lambda_l$). The dependence of f on q and ν can be found in Figure 2 for a single-cycle seed laser of wavelength $\lambda_l = 2.1\ \mu$m and for a single period modulator.

An example of this energy modulation can be found in Figure 3 where the modulator parameters were optimized to produce an amplitude of $\Delta\gamma = 20$ with a laser energy of $A_L \sim 360\ \mu$J. The choice in the seed laser wavelength, duration and number of modulator periods are crucial to differentiating the slope of the energy chirp near the zero crossing phase ($s \sim 6\mu$m) from the slope of the chirp in the regions immediately adjacent ($s \sim 4, 8\mu$m). Additionally, the choice in seed laser wavelength was motivated by the progress that has been made in recent years in obtaining carrier-envelope-phase-stable single-cycle pulses in this wavelength region [12]. There is a large and linear energy energy chirp around $s \sim 6\mu$m parameterized by $\alpha_c = d\gamma/ds \sim 2\pi\Delta\gamma/\lambda_l$. As previously mentioned, gain degradation due to an energy chirp along the electron beam longitudinal profile can be compensated by appropriately tapering the undulator. This taper is given analytically by:

$$\frac{dK}{dz} = \frac{1}{K_0}\left(1 + \frac{K_0^2}{2}\right)^2 \frac{\alpha_c}{\gamma_0^3}, \quad (3)$$
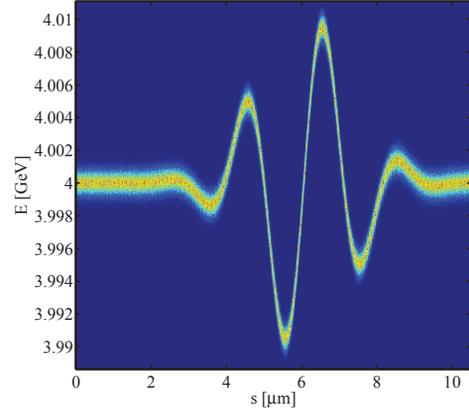
Figure 3: The longitudinal phase space near an energy modulation using a single-cycle $\lambda = 2.1\mu$m laser in a single period modulator.

where K_0 and γ_0 indicate the initial undulator parameter and e-beam energy respectively. This undulator taper also suppresses gain where there is no conjugate energy chirp, leaving ample real estate along the electron beam longitudinal profile for additional radiative processes. The taper that produced the optimal pulse characteristics (longitudinally coherent, single-spike, large contrast with remainder of pulse) is shown in Figure 4, which was $\sim 80\%$ of the theoretically predicted value.
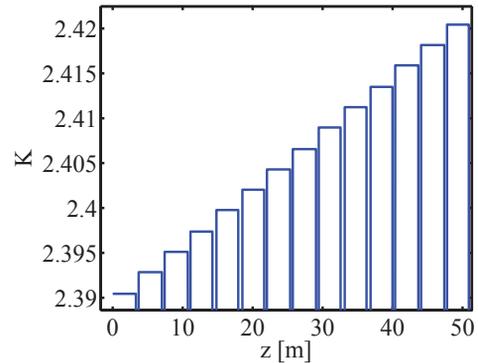
Figure 4: Undulator parameter along the undulator indicating the optimal taper to compensate for the energy modulation with $\Delta\gamma = 20$.

NUMERICAL SIMULATIONS

The FEL simulation code GENESIS was used to evaluate the performance of the chirp and taper combination in the context of the LCLS-II design project under ideal conditions. The results of twenty independent SASE simulations are shown in Figure 5 in the temporal and spectral domains. The longitudinal profile is dominated by a single spike of radiation in the gain compensation region that is > 2 orders

of magnitude larger than radiation that has been suppressed by the taper. There is a small time and energy jitter that
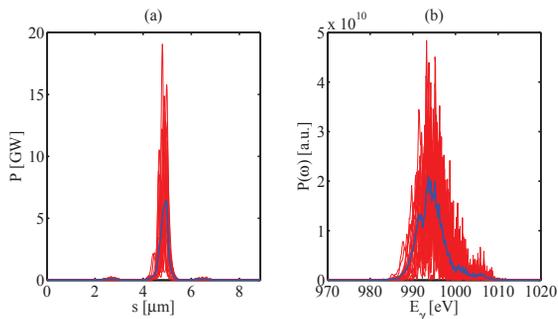
Figure 5: Power (left) and spectrum (right) of twenty independent simulations (red) and their average values (blue).

is associated with SASE and the start-up of radiation from shot-noise as illustrated in Figure 6. The left plot shows a "waterfall" of the longitudinal power profile for the twenty simulations separated on the y-axis by 10 GW. A small temporal jitter is evident. This is perhaps more clearly illustrated on the right, which is a scatter plot showing the pulse energy and arrival time deviations from the average value for the twenty independent SASE runs. The standard deviation for the temporal jitter distribution is only ~ 0.26 fs and for the energy jitter is $\sim 1.4 \mu$J.
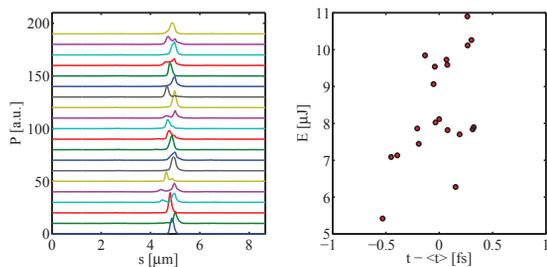
Figure 6: Longitudinal power (separated by 10 GW) (left) and a time and energy jitter distribution for twenty independent simulations.

It is useful, at this point, to analyze the pulse characteristics of a typical SASE simulation. The longitudinal profiles in the temporal and spectral domains are illustrated in Figure 7. The right plot shows the spectrum at saturation where the FWHM of $\Delta E_\gamma \sim 4.4$ eV is much larger than the nominal SASE bandwidth of an unmodulated electron beam in an untapered undulator. This is a result of the very large e-beam energy chirp, which produces a chirped FEL pulse and is manifested as a large quadratic spectral phase. The left plot shows the saturated FEL power (blue) in relation to the initial (green) and final (red) slice energies. The electrons clearly only give significant energy to the radiation where the undulator taper compensates for the electron beam energy chirp. This is also clearly illustrated in Figure 8, which
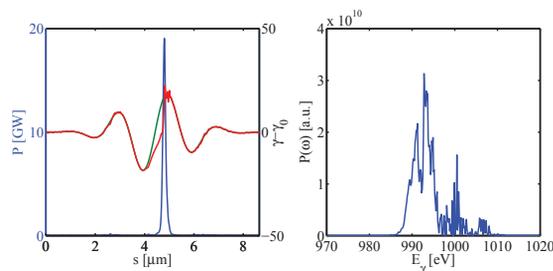
Figure 7: Power (blue), initial (green) and final (red) slice energy from the nominal resonance energy (left) and spectrum (right) of a typical simulation.

shows the power as a function of the electron beam coordinate (s, x-axis) and the distance along the undulator (z, y-axis). This figure also illustrates how the undulator taper suppresses the gain where it is not compensated by an appropriate energy chirp ($s \sim 0 - 2, 6 - 8 \mu$m). The peak power for the pulse illustrated in Figure 7 is $P_{pk} \sim 19$ GW while the FWHM temporal duration is $\Delta t \sim 0.42$ fs, corresponding to an energy of $E = 9.8 \mu$J and $\sim 6 \times 10^{10}$ photons. The FWHM
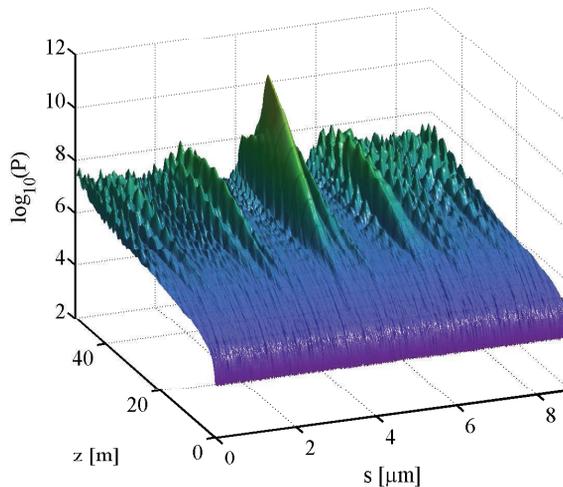
Figure 8: Power ($\log_{10}$ scale) as a function of s (electron beam coordinate) and z (undulator distance) showing the amplification of a single longitudinally coherent mode.

time-bandwidth product of this pulse is TBP~ 1.9 eV-fs and is very near the Fourier-transform limit. This pulse, however, is certainly not Gaussian, and so this number should be regarded carefully. Most pulses have a TBP of $3 - 5$ times the Fourier-transform limit. This is a direct consequence of the chirped nature of the FEL radiation, which is clearly illustrated by the on-axis, near field Wigner transform slightly before (left) and at saturation (right) shown in Figure 9. It should be noted that the Wigner transform here is dominated by a single coherent region. This particular pulse shows bandwidth growth and pulse compression as the pulse reaches saturation and slips forward onto the crest of

the electron beam energy modulation (see Figure 7) where the energy chirp is smaller and nonlinear.
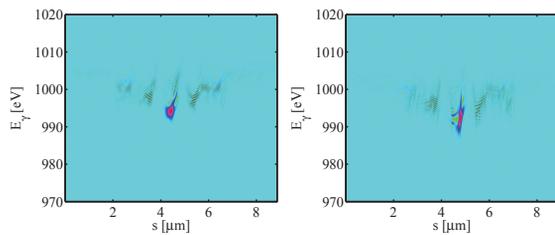
Figure 9: The on-axis, near field Wigner transform of the FEL pulse slightly before (left) and at saturation (right).

CONCLUSION

In conclusion, the selective amplification process initially proposed in [6] is easily adaptable to LCLS-II type parameters. An added benefit to working in this regime is that the optimal seed laser used for the energy modulation is based on technology that has been, and is continuing to be, well developed. The addition to an FEL facility of a beamline capable of delivering soft x ray pulses suitable for FWM spectroscopies is sure to revolutionize x ray science.

ACKNOWLEDGMENT

REFERENCES

[1] P. Emma *et al.*, *Nat. Photon.* **4**, 641 (2010)

[2] T. Ishikawa *et al.*, *Nat. Photon.* **6**, 540 (2012)

[3] W. Ackermann *et al.*, *Nat. Photon.* **1**, 336 (2007)

[4] E. Allaria *et al.*, *Nat. Photon.* **6**, 699 (2012)

[5] J. Marangos, *Cont. Phys.* **52**, 551 (2011)

[6] G. Marcus, G. Penn, A. A. Zholents, *Phys. Rev. Lett.* **113**, 024801 (2014)

[7] E. L. Saldin *et al.*, *Phys. Rev. ST Accel. Beams* **9**, 050702 (2006)

[8] L. Giannessi *et al.*, *Phys. Rev. Lett.* **106**, 144801 (2011)

[9] G. Marcus *et al.*, *Appl. Phys. Lett.* **101**, 134102 (2012)

[10] S. Reiche, *Nucl. Instr. Meth. Phys. Res. Sect. A* **429**, 243 (1999)

[11] A. A. Zholents, K. Holldack, in *Proceedings of the 28th International Free Electron Laser conference*, Berlin, Germany, 2008

[12] Y. Deng *et al.*, *Opt. Lett.* **37**, 4973 (2012)